Article

Comparison of Microstructures of Magnetite Reduced by H_2 and CO under Microwave Field

Meijie Zhou, Liqun Ai, Lukuo Hong *, Caijiao Sun, Yipang Yuan and Shuai Tong

College of Metallurgy and Energy, North China University of Science and Technology, Tangshan 063210, China; zhoumeijie0311@163.com (M.Z.); ailiqun@ncst.edu.cn (L.A.); 15032900376@163.com (C.S.); d202110284@xs.ustb.edu.cn (Y.Y.); ts961109@163.com (S.T.)
* Correspondence: honglk@ncst.edu.cn

Abstract: The reduction of magnetite in H_2 and CO atmospheres was compared using a microwave-heating technique. The reduction of magnetite in a mixed H_2 + CO atmosphere was compared with respect to the effects of a microwave field and a conventional field. Microstructural changes were observed using an electron microscope. The results show that the metallization rate and reduction degree of the H_2-reduced magnetite are much higher than those of the magnetite reduced by CO at 900–1100 °C. The Fe phase generated by H_2 reduction forms a cavity structure, and the Fe phase generated by CO reduction forms a dense block. Under conventional heating conditions, the higher the H_2 content in a pure CO atmosphere, the better the reduction effect. Under the effect of a microwave field, the atmosphere with the highest reduction rate was 50% H_2 + 50% CO. Compared with conventional heating, the bubble holes formed by reduced iron in microwave field are larger under the same conditions.

Keywords: H_2 reduction; magnetite; microwave heating; microstructural characterization

1. Introduction

The steel industry is facing increasingly severe environmental and policy pressures regarding carbon emissions. The world's leading steel manufacturers have incorporated carbon reduction into their national development strategies since the beginning of the 21st century. The existing approach to iron production is essentially a "carbon metallurgy" process using a carbon base as a reducing agent and a heat source. Exploring more innovative methods and breakthrough technologies is of great significance with respect to achieving ultra-low carbon emissions in the ironmaking stage. The rational use of H_2 in the process of ironmaking has a more significant effect on reducing energy consumption and CO_2 emissions. People continue to carry out experimental research on and theoretical simulations of various iron ore products (pellets, sinter, ore powder) under various atmospheres [1–6]. It is generally believed that the reaction rate and diffusion capacity of iron ore or pellets under a CO reduction atmosphere are much lower than those under the conditions relating to H_2 [7–11]. In cases of the same reduction degree, the direct reduced iron (DRI) yield of H_2 is lower than that of CO. The existing direct reduction process has a low production capacity, and its reduction temperature cannot be higher than 850°C (with this limit being imposed by sintering at high temperature).

Microwave processing has the characteristics of high-efficiency electric–thermal conversion, selective heating, volumetric heating, and an inverse thermal gradient. Furthermore, many experimental results have shown that microwaves enhance diffusion and reaction [12,13]. The "electric-hydrogen combination" model, which uses hydrogen instead of carbon for efficient reduction and electricity instead of carbon for a heat supply, is one method for eliminating carbon emission pressure. Microwave treatment enhances the permeability of a reaction gas and circumvents the premature closure of surface pores under a conventional thermal field [14]. Microwave radiation can change the thermodynamic

equilibrium [15,16], and it has a significant impact on the rate of chemical reaction and diffusion [17,18]. At present, the microwave heating reduction of iron ore has become a focus of solid carbothermal reduction research. Stir [19] studied the reduction of magnetite by carbon black under microwave radiation at 1050–1100 °C using online time-resolved XRD. The reduction of Fe_3O_4 is governed by a phase boundary reaction. The dynamic aggregation of cation vacancies and structural defects affects the kinetics of FeO's reduction to porous Fe. Amini A [20] studied the effect of the ratio of magnetite particle size to microwave penetration depth on the H_2 reduction reaction behavior. The results showed that the reduction effect of large particles (>40 μm) is better than that of small particles. However, there are few reports on the micro-morphology of the H_2/CO reduction of magnetite under a microwave field. This manuscript compares the reduction effect and microstructures of magnetite processed using microwave-heating technology under different conditions in H_2 and CO atmospheres. The reduction effect and microstructural differences of magnetite in a mixed H_2 + CO atmosphere influenced by a microwave field and a conventional field were compared.

2. Experimental Work

2.1. Experimental Equipment

The microwave-heating instrument used in this experiment was a WBMW-G4 tubular microwave-heating furnace (Tangshan Renshi Juyuan Microwave Instrument, Tangshan, China). The main components used are as follows: a heating furnace, a controllable atmosphere cabinet, a mixing box, and a high-temperature-resistant quartz tube. The temperature limit of the high-temperature-resistant quartz tube was ≤1500 °C, and its dimensions were Φ30 × 1000 mm. The heating constant temperature zone was 300 mm. The frequency of this furnace is 2.45 GHz, its power level is 4 kW, and the heating rate applied was 20 °C/min. The experimental samples were placed in a corundum crucible (60 mm × 30 mm × 15 mm) without compaction. As shown in Figure 1., the gas flow rate control instrument was placed in front of the experimental furnace, allowing for the more accurate control of gas flow. The gasses used in the experiment were Ar, H_2, and CO with a purity of 99.9% provided by Tangshan Rong sheng Gas (Tangshan Renshi Juyuan Microwave Instrument, Tangshan, China). The total gas flow rate was 1660 mL/min, and the reducing gas was mixed with a protective gas (Ar) in different proportions. Argon gas from the same supplier with the same purity was used for purging before and after reduction. The conventional heating furnace used in the experiment has been employed in previous studies [21]. Magnetite powder was embedded in JZXM0232 conductive hot inlay (conductive material was a copper-based polymer). The embedding temperature was 140 °C, the holding time was 10 min, and the mold was removed after it had cooled to room temperature. Then, grinding and polishing were performed to observe the cross sections of the mineral powder particles. Scanning electron microscopy (SEM, TESCAN MIRA LMS, Tangshan, China) was used to collect microstructural observations.
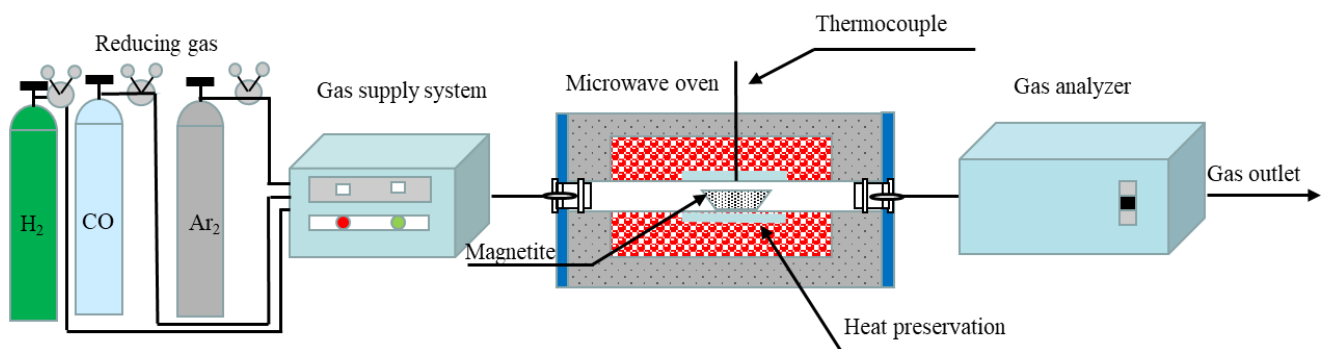

Figure 1. Microwave-heating furnace.

2.2. Experimental Raw Materials

Magnet mineral powder was used as a raw material in the experiment. The magnetite used in the experiment was acquired from a steel plant. The weight of each experimental sample was 15 g. An electronic balance (Changshu Shuang jie Testing Instrument Factory JJ224BC type, Changshu, China) was used to accurately weigh the samples. The samples were dried before the experiment. The drying temperature was 180 °C, and the drying time was 2 h. An X-ray diffractometer (Rigaku SmartLab SE, Tokyo, Japan) was used to quantitatively detect the magnetite concentrate used in the experiment. A table presenting the composition of the mineral powder is shown in Table 1. The magnet powder was dried at 180 °C for 4 hours using a drying instrument. The samples were tested using a Mastersizer 2000 laser particle size analyzer (Malvern, Shanghai, China) (Figure 2). The particle size of the magnet powder used in this experiment was between 10 μm and 200 μm, and the median particle size (D50) was 60.256 μm.

Table 1. Chemical composition of magnetite concentrate used in this work.

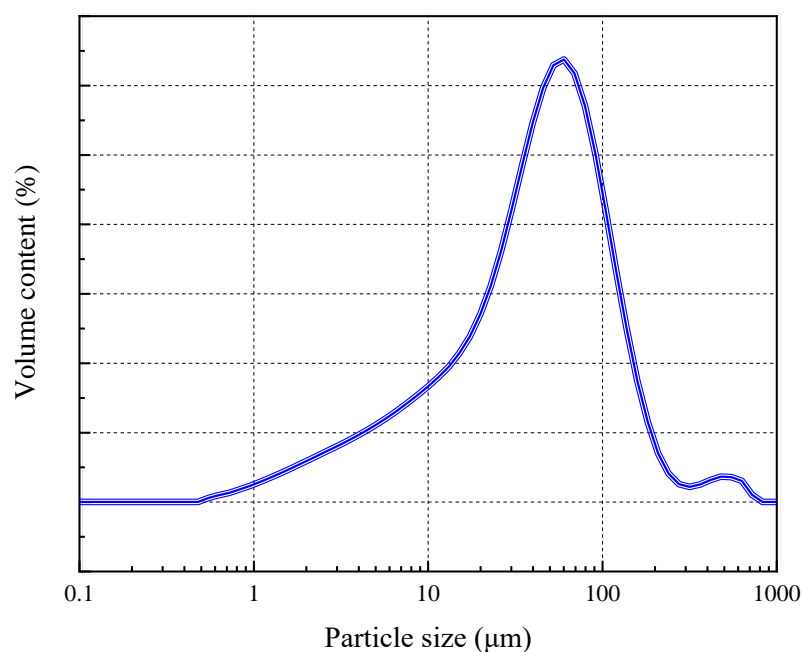| Component	Magnetite	Mica	Quartz	Amphibole
Weight percent	95.7%	1%	0.4%	2.9%

Figure 2. Magnetic powder particle distribution map.

3. Comparison of H₂/CO Reduction Effects under a Microwave Field

3.1. Calculation of Metallization Rate and Reduction Degree

Chemical titration was used to measure the metallic iron (MFe) and total iron (TFe) content, and then the metallization rate was calculated (Formula (1)):

$$m = \frac{\text{MFe}}{\text{TFe}} \tag{1}$$

where m is the degree of metallization, and TFe and MFe are the total iron and metallic iron fractions in the powder sample after reduction time t, respectively.

The weight loss measurement method was used to calculate weight loss, and then the reduction degree was obtained. Before the experiment, the undried magnetite sample was weighed and denoted as m_1. Then, the samples were dried and dehydrated. After drying, the samples were weighed and denoted as m_2. The reduced magnetite at the end of the

experiment was weighed again and denoted as m_3. $m_1 - m_2$, denoted as m_4, represent the mass of lost water. $m_4 - m_3$ signifies the mass of oxygen lost in the reduction process. The degree of reduction was calculated as follows:

$$x = \frac{m_4 - m_3}{m_4} \tag{2}$$

3.2. Reduction Effect Analysis

Figure 3a shows a comparison of the metallization rates of magnetite reduced by a microwave field. The reducing atmosphere employed consisted of 30% H_2-Ar, 30% CO-Ar, 60% H_2-Ar, and 60% CO-Ar. When the reduction atmosphere concentration was 30% and the temperature was 900–1100 °C, the metallization rate of H_2 reduction was 30–50% higher than that of CO reduction, and the maximum difference was 50% at 1050 °C. When the reduction atmosphere concentration was 60% and the temperature was 900–1100 °C, the metallization rate of H_2 reduction was 43–56% higher than that of CO reduction, and the maximum difference was 56% at 1100 °C. The higher the concentration of the reducing atmosphere and the higher the temperature, the more significant the metallization rate of the H_2-reduced magnetite compared to that of the CO-reduced magnetite. The metallization rate of the magnetite reduced for 40 min by 60% H_2-Ar at 1100 °C was 94%, and the reduction degree was close to 1. Under the same conditions, the metallization rate of CO reduction was 38%, and the reduction degree was 0.51.
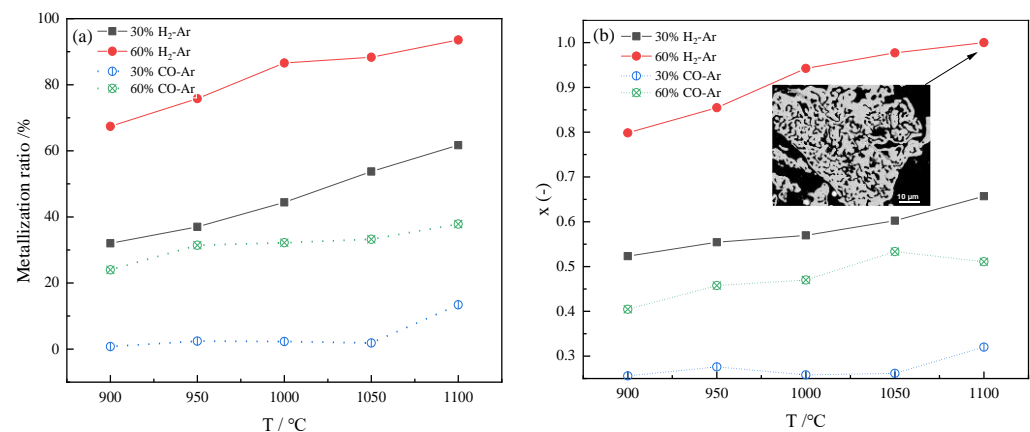

Figure 3. H_2 and CO reduction of magnetite under microwave field: (**a**) metallization ratio (**b**) reduction degree.

The effect of different H_2/CO concentrations on the degree of reduction of reduced magnetite under microwave heating between 900 and 1100 °C is shown in Figure 3b. At 1100 °C, the degree reduction of magnetite reaches 1, reaching 0.65 in 40 min with 60% and 30% H_2. At 1100 °C, the degree of reduction of magnetite reaches 0.51 and 0.32 in 40 min when reduced by 60% and 30% CO, respectively. With an increasing CO concentration, the degree of reduction of magnetite after reduction was significantly improved.

Similar conclusions have been obtained in studies of conventional fields. The rate at which solid iron oxide is reduced by H_2 can reach 5 to 10 times that of the CO reduction rate, and this effect is more significant when the temperature increases [22]. At 500 °C, the mutual diffusion coefficient of H_2/H_2O gas in iron-ore-sintered particles is 3 times that of CO/CO_2 [23]. In the molten state, the rate at which FeO is reduced by H_2 is 20 times that of the solid state [24]. Hydrogen molecules are much smaller than carbon monoxide molecules and can penetrate more deeply into the crystal structure of iron oxide, resulting in a greater degree of metallization. Both high temperature and increasing H_2% in the atmosphere help to improve the range of interfacial chemical reaction control and reduce the range of diffusion influence in the reduction process [6].

3.3. Microstructural Analysis

3.3.1. Magnetite Particle Morphology

The magnetite samples and epoxy resins were mounted with a mounting instrument and then polished. The morphology of the particles was observed using a scanning electron microscope (SEM). Figure 4a is an SEM image of the cross section of the magnetite particles. The gray regions correspond to Fe_3O_4, and the bright white regions correspond to the Cu in the inlay. Figure 4b depicts the original particle morphology.
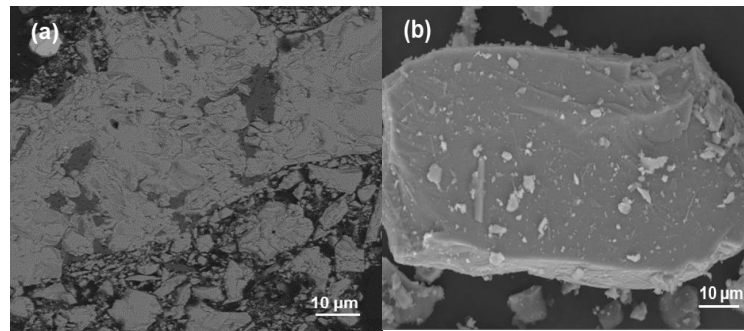

Figure 4. Morphology of magnetite particles. (**a**) SEM image of the cross section of the magnetite particles; (**b**) SEM image of magnetite particles.

3.3.2. The Effect of Different Temperatures

Figure 5 presents an image of the cross section of the magnetite particles reduced by 30% H_2-Ar and influenced by a microwave field. The reduction time was 40 min. In the figure, FeO is encircled by a reduced Fe phase. The metal iron layer that was reduced at a low temperature is dense. With the increase in temperature, the degree of reduction increases, the porous structure of metallic iron is obtained, and the iron layer is thickened. The reduction rate determines the formation of pores. The reaction rate increases with the increase in temperature. H_2 is more likely to penetrate the iron shell into FeOx. The result of gas permeation leads to the generation of bubbles, and the generation of bubbles further leads to tearing. The formation of water and its direct evaporation to the shell may be one of the reasons for the formation of pores.
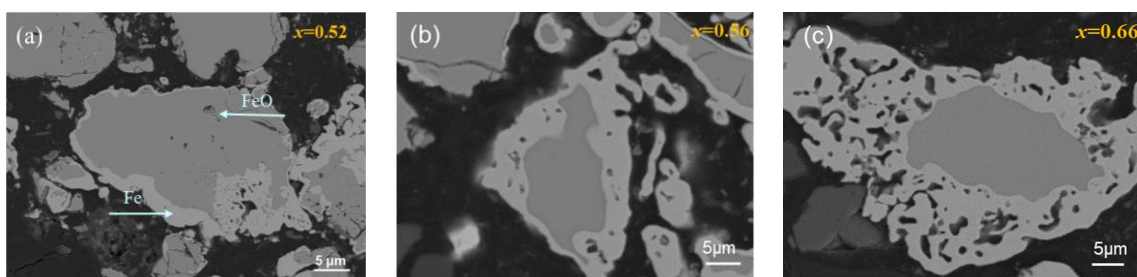

Figure 5. Microwave-field-enhanced 30%H_2-Ar reduction of magnetite at (**a**) 900 °C; (**b**) 1000 °C; (**c**) 1100 °C.

Figure 6 shows the image of 30% CO-Ar reduction magnetite in microwave field. The reduced metal iron layer is dense and blocky around the particles. The reduced metal iron layer is dense and non-porous. The metallic iron in the carbon monoxide reduction products is distributed in large aggregates in mineral particles. Figures 5 and 6 present the reduction degrees of the magnetite reduction products reduced by H_2 and CO at different temperatures, respectively. When comparing the microstructure of the H_2 reduction products in Figures 5 and 6, it can be seen that the reduction rate of CO is significantly slower than that of H_2 reduction. Under the same conditions, H_2 reduction produced more Fe than CO reduction. The unreduced FeO was completely surrounded

by the generated Fe phase, and the outer Fe phase was reduced to porous iron layer by layer. CO was reduced at the defect site and gradually expanded to form dense iron. There is no complete coating phase in the CO reduction product. S.P. Matthew [25] studied the surface morphology changes in the reduction process of dense Wüstite using an SEM detection method. Instabilities develop on the oxide surface prior to the growth of a dense iron layer. These instabilities develop into pores that continue to advance into the bulk oxide before advancing into the iron layer. During the reduction process, the formation of porous iron products at the interface mainly depends on the gas composition, reaction temperature, and mineral composition. It can be seen from Figure 5 that under a 30% H_2 atmosphere, the increase in temperature is beneficial to the formation of a porous structure, and the coating layer forms more easily at a low temperature (900 °C), while the small particle ore powder has almost no pores. In the reduction of ore powder by CO, the change in temperature and CO partial pressure could not produce either coated layered iron or pore structures. The above phenomenon shows that the formation of porous structures is affected by temperature and partial pressure. In addition, the effect of gas phase diffusion as a limiting factor of reduction is very critical. It is not easy to produce a porous structure when the gas phase diffusion is limited. In the process of H_2 reduction, hydrogen migrates to the interface, and an interface reaction occurs after the migration to the interface. The interface gradually shrinks with the extension of the reduction time. Since hydrogen has no orientation dependence, it advances as a whole at the reduction interface. CO reduction is reduced at the defect site, and the adsorption of CO responds accordingly. As the reduction proceeds, iron diffuses at the defect site, thereby forming a dense iron block. In the process of CO reduction, a carbon evolution reaction was more likely to occur at a low temperature in the temperature range of this experiment [26]. Therefore, the carbon content produced at 900 °C was relatively high. The resulting reduction product has high hardness and is easy to break. The reduction product is obviously broken at 900 °C.
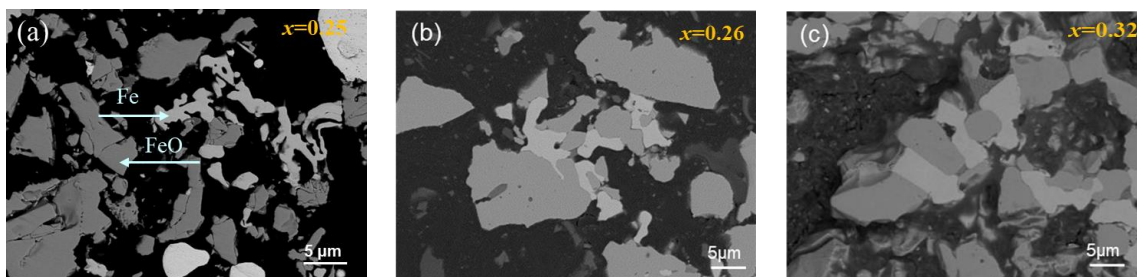

Figure 6. Microwave-field-enhanced 30%CO-Ar reduction of magnetite at (**a**) 900 °C; (**b**) 1000 °C; (**c**) 1100 °C.

In addition, the appearance of pores on the particle surface is conducive to the diffusion of the gas generated by the reaction to the interface for the reaction and the expulsion of the product gas. Zhan D [27] investigated the reduction of fine iron ore in a pure H_2 atmosphere. The angle between the surface and the Fe/Fe_{1-x} interface is smaller than the angle reduced in the pure CO. Therefore, the migration paths of $V^{//}_{Fe}$ and $2e^-$ in pure H_2 are shorter than those in pure CO, which causes the $Fe/Fe_{1-x}O$ interface to move faster in pure H_2. The results obtained by Yamashita [28] are consistent with this phenomenon, proving that when $Fe_{0.94}O$ is reduced at different temperatures and different reduction potentials, if the angle between the surface and the reaction interface is small, the migration speed of $V^{//}_{Fe}$ and $2e^-$ will increase, and the moving speed of the $Fe/Fe_{0.94}O$ interface will also increase. As shown in Figure 7, the microstructure of the particles after reduction at 1000 °C for 40 min. The mineral particles after H_2 reduction are porous honeycomb. The interconnected pore structure allows the gas to continuously enter the reaction interface from the sample surface through the product layer. However, there are many iron whiskers on the surface of the mineral after CO reduction, and the whiskers and dense layer are not conducive to efficient reduction.
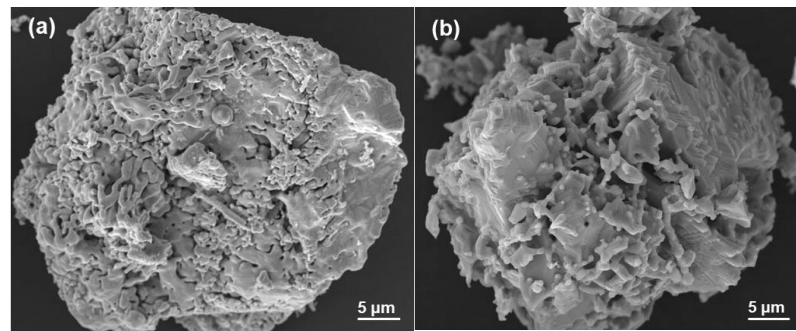
Figure 7. Microstructure of magnetite particles: (**a**) 30% H_2-Ar; (**b**) 30% CO-Ar.

4. Reduction of Magnetite by H_2 + CO Mixed Gas in Microwave Field

4.1. Reduction Effect Analysis

For the analysis of microwave heating and conventional heating at 1000 °C under the conditions of a H_2 + CO gas mixture employed for the reduction of magnetite, the following reducing atmospheres were used: 100% CO, 30% H_2 + 70% CO, 40% H_2 + 60% CO, 50% H_2 + 50% CO, 60% H_2 + 40% CO, 70% H_2 + 30% CO, and 100% H_2. Figure 8a shows that under conventional heating experimental conditions, the atmosphere with the lowest reduction degree was 100% CO. As long as H_2 was added in a pure CO atmosphere, the reduction effect was higher than that in a pure CO atmosphere, and the higher the H_2 content, the better the reduction effect. The reason for this involves the deposition of carbon. The presence of a small amount of CO can provide energy to the H_2-reduced iron ore, making the internal temperature of the mineral particles slightly higher than that of pellets without CO, which is conducive to reducing the interfacial chemical resistance of H_2 reduction. Geassy [29] investigated the reduction of Fe_2O_3 compacts using a H_2 + CO mixture in the temperature range of 700–1100 °C. Adding H_2 to CO can increase the reduction rate. The reduction rate of pure H_2 gas is faster than that of pure CO. Moon [30] investigated the reduction kinetics of hematite compacted at 800 °C and 950 °C with H_2 + CO mixtures using a thermogravimetric analyzer. The reaction rate increased with the increase in the H_2 content in the mixture. Olsson RG [31] showed that low concentrations of hydrogen also greatly increased the decomposition rate of CO, which might have been due to the catalytic effect of adsorbing hydrogen on iron. At high concentrations of hydrogen, the carbon deposition rate slows down due to the following reverse reaction: $H_2O + C \rightarrow H_2 + CO$.
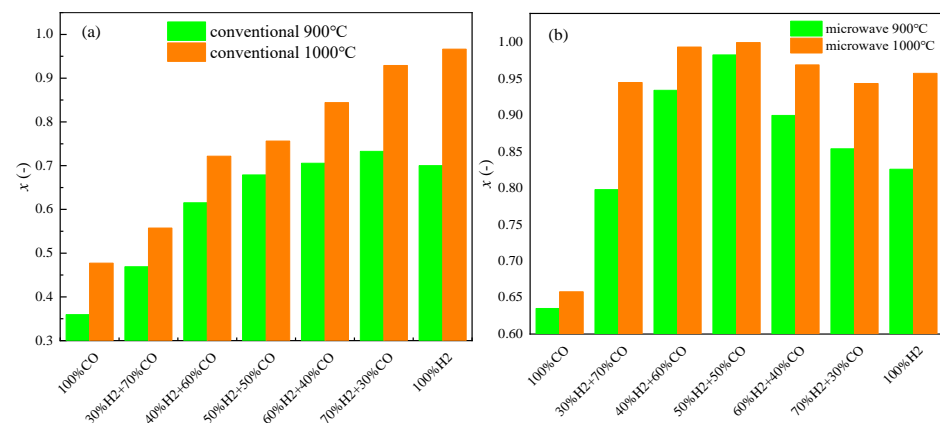

Figure 8. Reduction degree of samples during (**a**) conventional heating at 1000 °C and (**b**) microwave heating at 1000 °C.

Under a microwave field, it is not the case that the more H_2 added to the CO atmosphere, the better the reduction effect. The atmosphere with the highest reduction was 50% H_2 + 50% CO (Figure 8b). The reason for this finding is most likely that CO

changes the partial pressure of the atmosphere. CO and H_2O are polar molecules, and polar molecules are susceptible to microwave radiation, which changes the balance of $CO + H_2O \rightarrow H_2 + CO_2$, making the reduction reaction continue.

4.2. Microstructural Observation

Figures 9 and 10 show microstructural images of magnetite reduced by a mixed $H_2 + CO$ atmosphere under a microwave field and conventional field, respectively. The edge of the Fe layer reduced by pure H_2 under a microwave field is thicker, and the Fe layer reduced by 60% H_2 + 40% CO is highly dispersed. Even if the particles are relatively small, the reduced Fe is highly dispersed. That is, the pores generated by the reduction of mineral powder particles with a high reduction degree are more dispersed. Compared with conventional heating, the bubble holes formed by reduced iron under a microwave field are larger under the same conditions.
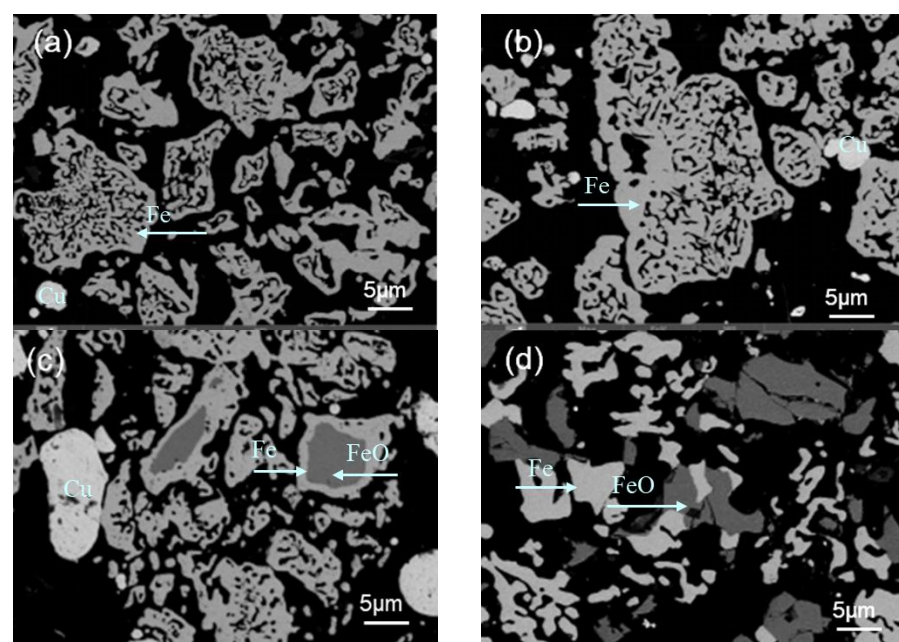

Figure 9. Microwave-field-enhanced reduction of magnetite at 1000 °C by (**a**) 40% H_2 + 60% CO; (**b**) 60% H_2 + 40% CO; (**c**) H_2 100%; (**d**) CO 100%.

In the pure CO-reduced magnetite, the Fe phase in the microwave field forms blocks, while the Fe phase in the conventional field forms strips. When CO is added to the H_2 atmosphere under microwave heating, the reduction products swell. The more CO that is added, the more serious the degree of swelling. Additionally, 100% CO reduction ore powder will undergo severe swelling. Under the conventional field of CO reduction, swelling is not obvious. The swelling of magnetite during the reduction process is attributed to the tearing of the iron layer and the swelling of the ore layer caused by the increase in internal pressure in the void of the Wüstite/Fe phase boundary [32]. Swelling is the process of reducing product cracking. When the reduction degree is low, a high degree of crack swelling occurs. With the increase in the reduction degree, fragmentation enhances, and swelling weakens. The reason for the rapid swelling under microwave radiation is that the growth rate of the iron phase is fast. Microwaves increase swelling and cracking, and the addition of hydrogen weakens this behavior. When H_2 is added to CO, CO induces reductive swelling, swelling, and even stripping, while H_2 guarantees diffusion and reduction rates. Therefore, the reduction degree of H_2 and CO in the microwave field is higher than that of pure H_2. Microwave treatment enhances the permeability of reaction gasses and circumvents the premature closure of surface pores under conventional thermal fields [33]. A microwave has the effect of accelerating reaction and diffusion,

and when the reaction rate is low, it will accelerate diffusion sintering. Therefore, the iron phase topography is smoother, and the external morphology of the raw ore is no longer maintained.
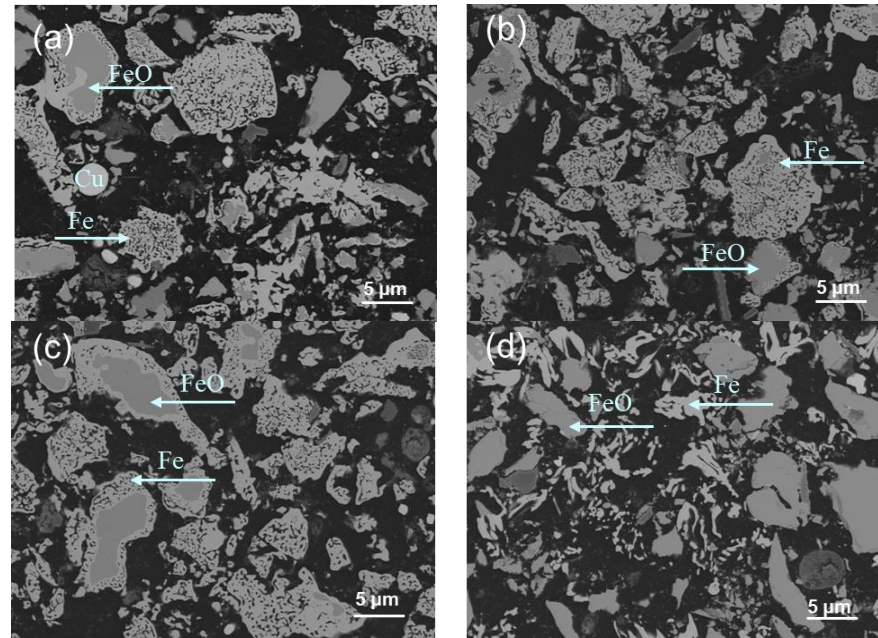

Figure 10. Magnetite was reduced under conventional field at 1000 °C by (**a**) 40% H_2 + 60% CO; (**b**) 60% H_2 + 40% CO; (**c**) H_2 100%; (**d**) CO 100%.

5. Conclusions

(1) The effects of the H_2 and CO reduction of magnetite under a microwave field were compared. Under a microwave field, the metallization rate of the H_2-reduced magnetite was 56% higher than that of CO at a high temperature. The metallization rate of magnetite reduced for 40 min by 60% H_2-Ar at 1100 °C was 94%, and the reduction degree was close to 1. Under the same conditions, the metallization rate of CO reduction was 38%, and the reduction degree was 0.51.

(2) The microscopic morphologies of the particles' cross sections were observed. Under the condition of a 30% H_2 atmosphere, the increase in temperature was beneficial to the formation of a porous structure, and the coating layer was more easily formed at a low temperature (900 °C), while the small particle ore powder had almost no pores. For the reduction of ore powder by CO, the change in temperature and CO partial pressure produced neither coated layered iron nor pore structures. The formation of porous structures was affected by temperature and partial pressure. In addition, the effect of gas phase diffusion as a limiting factor of reduction is very critical. It is not easy to produce a porous structure when the degree of gas phase diffusion is limited.

(3) The microstructures of the particles were observed. The mineral particles after H_2 reduction had a porous honeycomb shape. The interconnected pore structure allowed the gas to continuously enter the reaction interface from the sample surface through the product layer. However, there were many iron whiskers on the surfaces of the minerals after CO reduction, and the whiskers and dense layer were not conducive to efficient reduction.

(4) The reduction of magnetite under a microwave field and a conventional field in a H_2 + CO mixed atmosphere was observed. Under conventional heating experimental conditions, as long as H_2 was added in a pure CO atmosphere, the higher the H_2 content, the better the reduction effect. Under a microwave field, the atmosphere with the highest reduction rate was 50% H_2 + 50% CO.

References

1. De Castro, J.A.; de Medeiros, G.A.; da Silva, L.M.; Ferreira, I.L.; de Campos, M.F.; de Oliveira, E.M. A Numerical Study of Scenarios for the Substitution of Pulverized Coal Injection by Blast Furnace Gas Enriched by Hydrogen and Oxygen Aiming at a Reduction in CO_2 Emissions in the Blast Furnace Process. *Metals* **2023**, *13*, 927. [CrossRef]

2. Liu, D.; Wang, X.; Zhang, J.; Liu, Z.; Jiao, K.; Liu, X.; Wang, R. Study on the controlling steps and reduction kinetics of iron oxide briquettes with CO-H_2mixtures. *Met. Res. Technol.* **2017**, *114*, 611. [CrossRef]

3. Yi, L.; Zhang, N.; Liang, Z.; Wang, L.; Xiao, H.; Huang, Z. Coal ash induced ring formation in a pilot scale rotary kiln for low-grade iron ore direct reduction process: Characterization and mechanism. *Fuel* **2022**, *310*, 122342. [CrossRef]

4. Elahidoost, H.; Sheibani, S.; Raygan, S.; Hosseini, L.; Esmaeili, N. Mechanism of magnetite iron ore concentrate morphology affecting the pellet induration process. *Adv. Powder Technol.* **2022**, *33*, 103883. [CrossRef]

5. Rane, K.; Date, P.; Srivatsan, T.S. Influence of Material and Process Parameters on Reduction-Swelling Characteristics of Sintered Iron Pellets. *Metals* **2023**, *13*, 141. [CrossRef]

6. Mendoza, S.; Yin, B.H.; Zhang, A.; Bumby, C.W. Pelletization and sintering of New Zealand titanomagnetite ironsand. *Adv. Powder Technol.* **2022**, *33*, 103837. [CrossRef]

7. Lu, F.; Wen, L.; Zhao, Y.; Zhong, H.; Xu, J.; Zhang, S.; Yang, Z. The competitive adsorption behavior of CO and H_2 molecules on FeO surface in the reduction pro-cess-ScienceDirect. *Int. J. Hydrogen Energy* **2019**, *44*, 6427–6436. [CrossRef]

8. Ngoy, D.; Sukhomlinov, D.; Tangstad, M. Pre-reduction Behaviour of Manganese Ores in H_2 and CO Containing Gases. *ISIJ Int.* **2020**, *60*, 2325–2331. [CrossRef]

9. Scharm, C.; Küster, F.; Laabs, M.; Huang, Q.; Volkova, O.; Reinmöller, M.; Guhl, S.; Meyer, B. Direct reduction of iron ore pellets by H_2 and CO: In-situ investigation of the structural transformation and reduction progression caused by atmosphere and temperature. *Miner. Eng.* **2022**, *180*, 107459. [CrossRef]

10. Spreitzer, D.; Schenk, J. Iron Ore Reduction by Hydrogen Using a Laboratory Scale Fluidized Bed Reactor: Kinetic Investigation—Experimental Setup and Method for Determination. *Met. Mater. Trans. B* **2019**, *50*, 2471–2484. [CrossRef]

11. Farjas, J.; Roura, P. Modification of the Kolmogorov–Johnson–Mehl–Avrami rate equation for non-isothermal experiments and its analytical solution. *Acta Mater.* **2006**, *54*, 5573–5579. [CrossRef]

12. Ferrari, A.; Hunt, J.; Lita, A.; Ashleyl, B.; Stiegmanl, A.E. Microwave-Specific Effects on the Equilibrium Constants and Thermo-dynamics of the Steam−Carbon and Related Reactions. *Indian J. Chem. A* **2014**, *118*, 9346–9356. [CrossRef]

13. Malhotra, A.; Hosseini, M.; Zaferani, S.H.; Hall, M.; Vashaee, D. Enhancement of Diffusion, Densification and Solid-State Reactions in Dielectric Materials Due to Interfacial Interaction of Microwave Radiation: Theory and Experiment. *ACS Appl. Mater. Interfaces* **2020**, *12*, 50941–50952. [CrossRef] [PubMed]

14. Zhou, J.; Xu, W.; You, Z.; Wang, Z.; Luo, Y.; Gao, L.; Yin, C.; Peng, R.; Lan, L. A New Type of Power energy for Accelerating Chemical Reactions: The Nature of a Microwave-driving Force for Accelerating Chemical Reactions. *Sci. Rep.* **2016**, *6*, 25149. [CrossRef]

15. Arshad, F.; Munir, A.; Tahir, A.; Hussain, S.Z.; Jilani, A.; Hussain, A.; Ullah, N.; Sher, F.; Hussain, I. Microwave-assisted growth of spherical core-shell NiFe LDH@CuxO nanostructures for electrocatalytic water oxidation reaction. *Int. J. Hydrogen Energy* **2023**, *48*, 4719–4727. [CrossRef]

16. He, Y.; Liu, J.; Chen, C.-L.; Zhuang, C.-L. Carbothermal reduction characteristics of oxidized Mn ore through conventional heating and microwave heating. *Int. J. Miner. Met. Mater.* **2021**, *28*, 221–230. [CrossRef]

17. Wen, M.; Liu, Y.Q.; Wang, X.N. Reaction Kinetics of Niobium Concentrate Microwave Carbothermal Reduction. *Non-Ferr. Met.* **2022**, *7*, 74–81.

18. Binner, J.G.P.; Al-Dawery, I.A.H. Microwave melt texturing of bulk YBCO superconductors. *Supercond. Sci. Technol.* **1998**, *11*, 1230–1236. [CrossRef]

19. Stir, M.; Ishizaki, K.; Vaucher, S.; Nicula, R. Mechanism and kinetics of the reduction of magnetite to iron during heating in a microwave E-field maximum. *J. Appl. Phys.* **2009**, *105*, 124901. [CrossRef]

20. Amini, A.; Ohno, K.-I.; Maeda, T.; Kunitomo, K. Effect of the Ratio of Magnetite Particle Size to Microwave Penetration Depth on Reduction Reaction Behaviour by H_2. *Sci. Rep.* **2018**, *8*, 15023. [CrossRef]

21. Sun, C.; Ai, L.; Hong, L.; Li, Y. Study on solid state steelmaking from thin cast iron sheets through decarburization in H_2O–H_2. *Ironmak. Steelmak.* **2019**, *47*, 1015–1021. [CrossRef]

22. Pineau, A.; Kanari, N.; Gaballah, I. Kinetics of reduction of iron oxides by H_2: Part I: Low temperature reduction of hematite. *Thermochim. Acta* **2006**, *447*, 89–100. [CrossRef]

23. Murakami, T.; Kamiya, Y.; Kodaira, T.; Kasai, E. Reduction Disintegration Behavior of Iron Ore Sinter under High H_2 and H_2O Conditions. *ISIJ Int.* **2012**, *52*, 1447–1453. [CrossRef]

24. Pineau, A.; Kanari, N.; Gaballah, I. Kinetics of reduction of iron oxides by H_2: Part II. Low temperature reduction of magnetite. *Thermochim. Acta* **2007**, *456*, 75–88. [CrossRef]

25. Matthew, S.P.; Cho, T.R.; Hayes, P.C. Mechanisms of porous iron growth on wustite and magnetite during gaseous reduction. *Met. Trans. B* **1990**, *21*, 733–741. [CrossRef]

26. Nishihiro, K.; Maeda, T.; Ohno, K.-I.; Kunitomo, K. Effect of H_2 Concentration on Carbon Deposition Reaction by CO–H_2 Gas Mixture at 773 K to 973 K. *ISIJ Int.* **2019**, *59*, 634–642. [CrossRef]

27. Du, Z.; Zhu, Q.; Fan, C.; Pan, F.; Li, H.; Xie, Z. Influence of reduction condition on the morphology of newly formed metallic iron during the fluid-ized bed reduction of fine iron ores and its corresponding agglomeration behavior. *Steel Res. Int.* **2016**, *87*, 789–797. [CrossRef]

28. Yamashita, T.; Nakada, T.; Nagata, K. In-Situ Observation of $Fe_{0.94}O$ Reduction at High Temperature with the Use of Optical Microscopy. *Met. Mater. Trans. B* **2007**, *38*, 185–191. [CrossRef]

29. Ei-Geassy, A.A.; Shehata, K.A.; Ezz, S.Y. Mechanism of Iron Oxide Reduction with Hydrogen/Carbon Monoxide Mixtures. *Trans. Iron Steel Inst. Jpn.* **1977**, *17*, 629–635. [CrossRef]

30. Moon, I.-J.; Rhee, C.-H.; Min, D.-J. Reduction of hematite compacts by H_2-CO gas mixtures. *Steel Res.* **1998**, *69*, 302–306. [CrossRef]

31. Olsson, R.G.; Turkdogan, E.T. Catalytic effect of iron on decomposition of carbon monoxide: II. Effect of additions of H_2, H_2O, CO_2, SO_2 and H_2S. *Met. Trans.* **1974**, *5*, 21–26. [CrossRef]

32. Kapelyushin, Y.; Sasaki, Y.; Zhang, J.; Jeong, S.; Ostrovski, O. Effects of Temperature and Gas Composition on Reduction and Swelling of Magnetite Concentrates. *Met. Mater. Trans. B* **2016**, *47*, 2263–2278. [CrossRef]

33. Skamser, D.J.; Johnson, D.L. Simulation of Hybrid Heating. *MRS Proc.* **1994**, *347*, 325. [CrossRef]